IOPscience iopscience.iop.org

Home Search Collections Journals About Contact us My IOPscience

On the spectral response measurement of multijunction solar cells

This content has been downloaded from IOPscience. Please scroll down to see the full text.

2017 Meas. Sci. Technol. 28 055203

(http://iopscience.iop.org/0957-0233/28/5/055203)

View the table of contents for this issue, or go to the journal homepage for more

Download details:

IP Address: 89.202.245.164
This content was downloaded on 10/04/2017 at 15:38

Please note that terms and conditions apply.

You may also be interested in:

Spectral response measurement of double-junction thin-film PV devices
Mauro Pravettoni, Roberto Galleano, Alessandro Virtuani et al.

On the spectral response of PV modules
J Y Ye, S Guo, T M Walsh et al.

Non-linearity measurements of solar cells with an LED-based combinatorial flux addition method
Behrang H Hamadani, Andrew Shore, John Roller et al.

Design of InP-based metamorphic high-efficiency five-junction solar cells for concentrated photovoltaics
Yong Huang and Hui Yang

Effects of 1.0–11.5 MeV Electron Irradiation on GaInP/GaAs/Ge Triple-junction Solar Cells for Space Applications
Wang Rong, Lu Ming, Yi Tian-Cheng et al.

Effects of 50 keV and 100 keV Proton Irradiation on GaInP/GaAs/Ge Triple-Junction Solar Cells
Wang Rong, Feng Zhao, Liu Yunhong et al.

Current–voltage and spectral-response characteristics of surface-activated-bonding-based InGaP/GaAs/Si hybrid triple-junction cells
Naoteru Shigekawa, Jianbo Liang, Ryusuke Onitsuka et al.

Quantum dot optoelectronic devices: lasers, photodetectors and solar cells
Jiang Wu, Siming Chen, Alwyn Seeds et al.

IOP Publishing Measurement Science and Technology
Meas. Sci. Technol. **28** (2017) 055203 (10pp) https://doi.org/10.1088/1361-6501/aa5749

On the spectral response measurement of multijunction solar cells

J García[1], H Socolovsky[1] and J Plá[1,2,3,4]

[1] Departamento Energía Solar, Gerencia Investigación y Aplicaciones, Comisión Nacional de Energía Atómica (CNEA), Av. General Paz 1499, 1650 San Martín, Provincia de Buenos Aires, Argentina
[2] Consejo Nacional de Investigaciones Científicas y Técnicas (CONICET), Godoy Cruz 2290, 1425, Provincia de Buenos Aires, Argentina

E-mail: jpla@tandar.cnea.gov.ar

Received 4 October 2016, revised 22 December 2016
Accepted for publication 6 January 2017
Published 6 April 2017

Abstract

This work presents particular aspects dealing with the measurement of the spectral response (SR) on multijunction solar cells, a tricky and somewhat complex issue. Here, we demonstrate the development of a facility to measure SR between 300 nm and 1900 nm on III–V solar cells for space applications, particularly oriented to measure large area triple junction (3J) InGaP/GaAs/Ge cells, although it can be utilized to measure other types of devices. The equipment is based on narrowband interference filters and a novel and low cost approach of two dichroic lamps as bias light source, used to select the subcell to be measured using suitable bandpass filters, whereas a simple incandescent halogen lamp is used to generate the monochromatic light beam. The signal is measured on an appropriate resistance inserted in a serial circuit using a lock-in amplifier. Measurement is fully automated, which allows operator independent results. Detailed studies performed on bias spectrum conditions and voltage biasing for these types of cell are showed, as well as a thorough treatment of the uncertainty and measurement error sources. Preliminary SR measurement results demonstrate the good performance of this setup. As an example, the results of the application of this setup to analyze radiation damage induced by 10 MeV protons are shown.

Keywords: spectral response, multijunction solar cell, space cells, radiation damage

(Some figures may appear in colour only in the online journal)

1. Introduction

The Solar Energy Department (DES) of the Argentine National Atomic Energy Commission (CNEA) performs R&D activities related to photovoltaic solar energy conversion for space and terrestrial applications. Different contracts subscribed between CNEA and the Argentine National Commission for Space Activities (CONAE) promoted the development of photovoltaic arrays for space applications. Activities in this field have included: development of computational codes for solar array design and performance prediction, test of solar devices in Argentine satellites, on-ground radiation damage experiments, and development of characterization and device simulation techniques, as reported elsewhere [1–8].

This work is focused on the spectral response (SR) measurement on monolithic multijunction solar cells; although the term 'spectral responsivity' appear sometimes in the specialized literature, we prefer to use the more extended denomination 'SR', understood as the current generated by a solar cell at a given monochromatic illumination at constant power, measured in the whole wavelength interval where the device has response. A number of relevant reports have been devoted to the measurement of the SR of photovoltaic devices. Most of these describe setups that employ either interference filters [9, 10] or a monochromator [11, 12]. The setup based on an array of interference filters offers the advantage of generating the monochromatic light source in a simple and inexpensive manner. On the other hand, the monochromator allows measurements with increased wavelength resolution that may not be strictly necessary for crystalline solid devices due to the

[3] Group website: www.tandar.cnea.gov.ar/grupos/solar.html
[4] Author to whom any correspondence should be addressed.

 © 2017 IOP Publishing Ltd Printed in the UK

smoothness of the SR(λ). A most recent alternative approach based on commercial LEDs (Light Emitting Diodes) as the monochromatic light source has been proposed for the measurement of a-Si devices with explicit limitations in both the active wavelength range and potential area of the solar cells under test [13]. Moreover, for large area a-Si modules it has been proposed a setup where an off-axis reflector projects the monochromatic beam on part of the module and the light bias is provided by a set of 24 quartz tungsten halogen (QTH) lamps and 5 power LEDs to give subcell selection [14].

The SR measurement is carried out by measuring both a calibrated reference cell and the cell under test (as described in [9]). The SR is then calculated according to:

$$\mathrm{SR}^{\mathrm{cel}}(\lambda) = \frac{A^{\mathrm{ref}}}{A^{\mathrm{cel}}} \cdot \frac{V^{\mathrm{cel}}(\lambda)}{V^{\mathrm{ref}}(\lambda)} \cdot \mathrm{SR}^{\mathrm{ref}}(\lambda) \qquad (1)$$

where V^{cel} and V^{ref} are the lock-in voltage readings that are proportional to the short-circuit current of the cell under test and the reference cell at the wavelength λ, respectively. A^{cel} and A^{ref} are the corresponding device areas of the cell and reference and $\mathrm{SR}^{\mathrm{ref}}$ is the absolute SR of the reference cell. It is important to consider that the absolute SR depends on the actual illuminated area. Therefore, the areas of the bus and fingers corresponding to the front contact must be subtracted from the total device area because they block light from reaching the cell. Any errors in area measurements are transferred directly to the absolute SR, so it is crucial to minimize them. It is also very important to consider the measurement error associated to the monochromatic beam spectral width. When a Xe lamp is used for the monochromatic light source, an inaccuracy originated in the asymmetrical beam profile has been reported [15]. The typical pronounced IR peaks of the Xe arc lamp generates a non symmetrical profile of the monochromatic beam when light passes through filters with a finite wavelength width, leading to errors in the SR estimation where the integral over all the wavelengths is performed. This type of error can be avoided using smooth spectrum lamps, like the one generated with a QTH lamp. Other possible contributions to the measurement error are extensively described by Emery *et al* [10], and they will be considered in the section 4.

SR measurements in multijunction solar cells have the additional difficulty of testing the monochromatic response of each junction by ensuring that the subcell under test limits the current of the entire cell. Therefore, it is highly important to use a bias light with the appropriate spectral content that makes the corresponding subcell to limit the current, as established in early papers that treated the issue [16–18]. Also, in some cases it is necessary to apply an external bias voltage that ensures the short-circuit condition of the subcell to be measured [19]. In general terms, the content of the light bias spectrum used in SR measurements have not been fully described in the literature. Just to mention a few, Haverkamp *et al* describes the use of seven high power LEDs in order to obtain different spectral conditions for subcell selection [20]. Winter *et al* [11] reports an array of 36 cold light mirror lamps with dichroic reflectors but no details on the spectral content are presented. The approach of Pravettoni *et al* [14] considers combinations of LEDs and QTH sources for subcell selection and also does not provide further details on the spectrum and intensity of the bias light. For the second part, the condition on the bias voltage is particularly relevant in the case of the Ge subcell when standard InGaP/GaAs/Ge triple junction cells are under study. Non optimized bias voltages have been reported to produce artifacts in the measurement and have been described in the work of Meusel *et al* [19]. When all the appropriate conditions are adjusted for each subcell, the equation (1) is then consecutively applied for the complete measurement.

In this work, a homemade equipment, initially designed to measure the SR of silicon solar cells (300–1100 nm) based on narrow band optical filters and a lock-in amplifier, was modified in order to measure III–V multijunction solar cells of monolithic structure. The complexity of the measurement and possible artifacts associated with the measurement mentioned above have been described in [10, 19]. Also, possible artifacts due to luminescent coupling depending on the bias voltage were outlined recently in the paper of Steiner and Geisz [21] and references there in. Another possibility to produce measurement artifacts, associated with low breakdown voltage cells, was pointed out by Barrigón *et al* [22]. Modifications in the optical setup and improvements in the electrical circuitry of the previous setup have enabled to perform SR measurements on III–V based solar cells of quite different areas, as showed in an early publication [23]. Also, the effect of the monochromatic beam asymmetrical shape is minimized using a quartz halogen tungsten lamp and 10 nm narrow band filters to define the monochromatic beam. Furthermore, a simplified and low cost approach for the bias light based on two dichroic lamps is employed and coupled to the appropriate band pass optical filters that emulate 1 sun spectra close to AM0 while subcell selection is performed in a very simple manner in comparison with other approaches by using an appropriate combination of optical bandpass filters. At the same time, irradiance conditions close to the cell operation ones (1367 W m^{-2}) are provided. Thus, the main aspect of the setup modification was to change the light bias to gain the ability to bring three appropriate spectra for the bias light to measure each subcell in triple junction (3J) InGaP/GaAs/Ge solar cells. A detailed description of the setup and the way of obtaining those spectra is presented. A second filter wheel was added to extend the range of the measurement from 1100 nm to 1900 nm in order to cover the full range of InGaP/GaAs/Ge cells response. The full details of the setup calibration are presented. Finally, the SR instrument setup is demonstrated in a practical application that evaluates the radiation damage by high energy proton irradiation onto a 3J InGaP/GaAs/Ge solar cell.

2. Optical setup

2.1. Monochromatic light

The monochromatic light is generated by a single 250 W QTH lamp fed by a stabilized DC (direct current) power source. An optical condenser is placed on the lamp beam pathway in order to focus the light onto the chopper blade and through the interference filters (figure 1). The filters of 10–15 nm

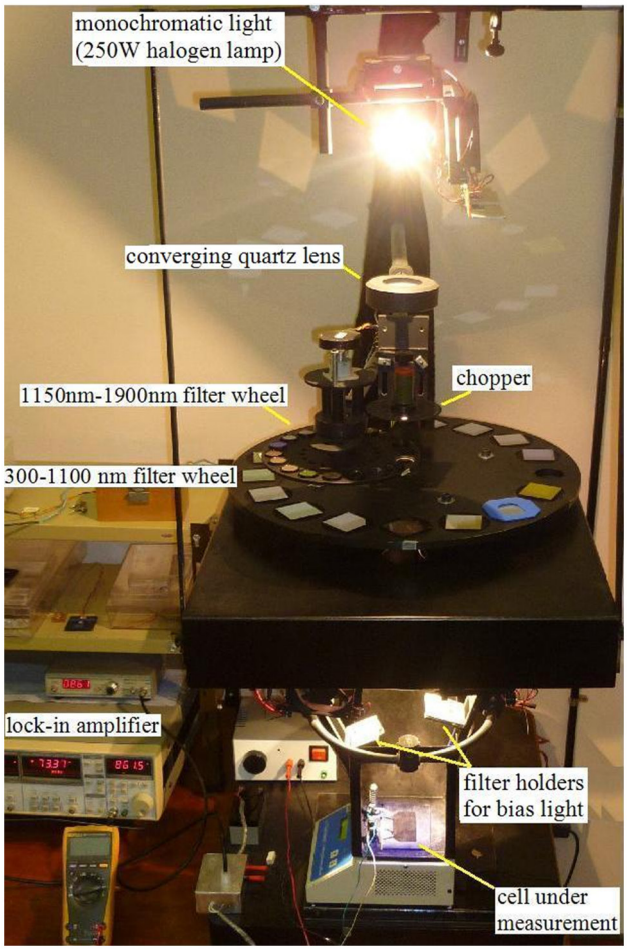

Figure 1. SR measurement equipment view.

bandwidths are mounted onto two rotating wheels. The first wheel introduces square $2'' \times 2''$ filters for the 300–1100 nm range and the second wheel extends the spectrum range into the infrared section (1150–1900 nm) with circular filters ($1''$ diameter). All filters were carefully chosen with central wavelengths in steps of 50 nm such that the spectrum covers 33 wavelengths between 300 nm and 1900 nm.

The light beam was modulated with a chopper situated at the focus of the optical condenser formed by two convergent quartz lenses. The size ratio between the image of the lamp filament formed by the condenser lens at the chopper plane and the size of the slot of the chopper blade defines the resulting monochromatic light waveform. In our case this waveform is not square, but triangular, which is better due to the minor harmonic content of the signal [24].

The extended spectrum of the QTH lamp is filtered by the narrow-band interference filters to produce the monochromatic beam. The resulting intensity of this beam is very small, which makes necessary the use of synchronous detection of the signal through a lock-in amplifier. The spectrum for almost all wavelengths available was measured with a spectrometer *Analytical Spectral Device Inc* model *FieldSpec Pro FR*, and later scaled using the integral intensity of the QTH lamp at the measurement plane given by a *Kipp&Zonen CMP 6 pyranometer*, so values of spectral irradiance were obtained. These values, integrated for all wavelengths, are presented in table 1.

Table 1. Estimated monochromatic beam irradiance at the plane of measurement for several wavelengths.

Wavelength (nm)	Irradiance (W m^{-2})	Wavelength (nm)	Irradiance (W m^{-2})
400	0.006	1200	0.055
450	0.013	1250	0.051
500	0.018	1300	0.050
550	0.038	1350	0.023
600	0.044	1400	0.053
650	0.062	1450	0.035
700	0.063	1500	0.044
750	0.110	1550	0.034
800	0.071	1600	0.030
850	0.090	1650	0.028
900	0.098	1700	0.023
950	0.104	1750	0.027
1000	0.091	1800	0.020
1050	0.076	1850	0.119
1100	0.098	1900	0.030
1150	0.048		

Resulting spectra of QTH and the filtered light are shown in figure 2, where the consistent relation (mediated by filters transmittance) between the peaks of the filtered light and the QTH spectrum is noticed.

According to the ASTM standard requirement, the spatial non-uniformity of the monochromatic light on the plane test must be less than $\pm 2.5\%$ [25]. The in-plane intensity distribution was measured with a calibrated Si sensor (6 mm^2 active area) connected to an appropriate resistor to bias it near short-circuit conditions (the voltage developed across the resistance was about 20 times lower than their V_{OC}). The measured uniformity can be observed in the figure 3, where it is shown an area of approximately 4 cm $\times$ 7.5 cm that meets the required uniformity (enough to measure a variety of formats and sizes of cells).

We performed a set of homogeneity measurements of the monochromatic beam for several filters and without filter (this is the case of figure 3), and we verified the homogeneity condition for all cases. However, the transmittance of the filters should be periodically checked in order to prevent changes due to filter aging degradation.

2.2. Bias light setup

As discussed above, bias light of triple junction cells is intended to expose the device under test close to standard working conditions while each subcell is selected. Bias light is produced by two 250 W dichroic lamps, individually fed with a stabilized DC power source (the sum of both lamps yield an irradiance of about twice the standard AM0 spectrum at the test plane). From now on, we will refer as AM0 the spectrum defined in the standard ASTM E490-00a [27]. Each lamp has a filter holder for short-pass, long-pass and other optical filters. The lamps spectra and the appropriate filters are combined to determine which subcell will limit the 3J current. In all cases, the short-circuit current generated is at a similar level to the operating short-circuit current under AM0 spectrum. The spatial uniformity

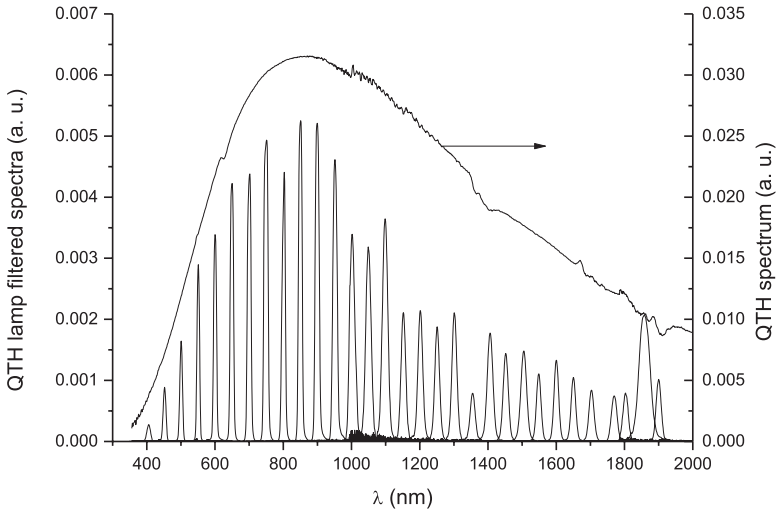

Figure 2. Measured spectra of QTH lamp and transmitted by the narrowband optical filters.

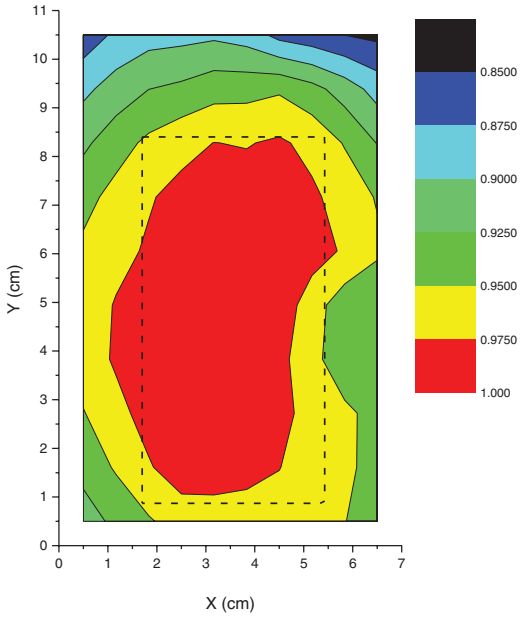

Figure 3. Intensity distribution of monochromatic light in normalized units at maximum intensity value. The rectangle defines an area of $4 \times 7.5\,\mathrm{cm}^2$ where the ASTM standard requirement is accomplished, enough to measure a large area commercial space solar cell.

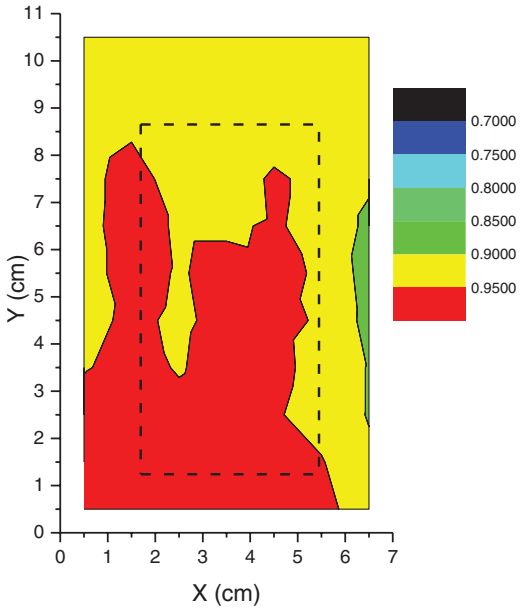

Figure 4. Intensity distribution of bias light in normalized units at maximum intensity value. The same rectangle depicted in figure 3 is shown as a reference.

of the combined light sources at the sample plane remains below $\pm 10\%$ according to the standard requirement mentioned in [25]. The spatial uniformity is depicted in the figure 4, where an area of approximately $10\,\mathrm{cm} \times 5.5\,\mathrm{cm}$ meets the required uniformity. Finally, ambient light and possible scattering of the beam arriving to the chopper blade were controlled using suitable optic confiners as observed in figure 1.

2.3. Bias light condition for each subcell

Given a lighting spectrum $E(\lambda)$, the short circuit current generated under light illumination by the subcell i is equal to the integral of the SR of the subcell $\mathrm{SR}^i(\lambda)$ multiplied by the spectral distribution, according to the equation (2):

$$J^i_{\mathrm{SC}} = \int \mathrm{SR}^i(\lambda) E(\lambda) \mathrm{d}\lambda \tag{2}$$

where the integral extends between the limits within which the amounts $\mathrm{SR}^i(\lambda)$ and $E(\lambda)$ are nonzero.

In the presented setup, the bias light spectrum can be modified by the interposition of band-pass filters, so that if $T(\lambda)$ is the spectral transmittance of the filter, the modified spectrum is $E_m(\lambda) = E(\lambda)T(\lambda)$. The setup has a set of band-pass filters (High and Low) $2''$ squared, with cutoff wavelengths between 400 nm and 750 nm. The transmittance of the band-pass filters was measured using a *Shimadzu* spectrophotometer UV–vis–IR. Neutral density filters are added to reduce the intensity uniformly throughout all wavelengths whenever necessary.

In order to solve equation (2) numerically to generate the suitable spectra for the bias light, several computer simulations were done using the dichroic lamps spectra (measured in the lab with a spectrometer *Analytical Spectral Device Inc* model *FieldSpec Pro FR* provided by CONAE), the filters transmittance and the standard SR of an InGaP/GaAs/Ge cell as obtained from [12]. The InGaP/GaAs/Ge cells were considered to work under AM0 spectrum such that the bias spectrum must resemble it closely with an irradiance of 1367 W m^{-2} (1 sun under standard conditions). For these conditions the top subcell (InGaP) limits the current. The remaining subcells, middle (GaAs) and bottom (Ge), were forced to limit current by imposing minor changes in the spectra.

Figure 5 depicts the different spectra employed in our setup that clearly resemble the AM0 spectrum. Top, Middle and Bottom stand for the spectra that force to limit the current by the Top, Middle, and Bottom cell respectively. The spectral radiation intensity integral was compared to 1 sun AM0 using a solar radiometer *Kipp & Zonen*, model *CM5*. This resulted in the following differences between the 1 sun AM0 spectrum and the measurement for each spectrum: for top cell selection, the irradiance respect to 1367 W m^{-2} is +10.9%, for middle cell selection is +23.4%, and finally +9.5% for bottom cell selection. Table 2 presents a comparison between the three spectra for cell selection and the AM0 spectrum, considering the 300–1900 nm range sectioned in 100 nm intervals. The spectral mismatch, calculated according to the ASTM standard E 927-91 [28] in the whole range of cell response (300–1900 nm), is shown in this table. The weight of each spectral section for all spectra is expressed as a percentage of the integral performed over the full spectrum (% of total), and the AM0 standard is considered as reference. The spectra comparison was realized considering relative values of the weight referred to the AM0 standard. The analysis of the data presented shows the spectral mismatch is in average lower than 30%, with the obvious exceptions dictated by the limited UV and IR irradiance of dichroic lamps, limitations of the spectrophotometer measurement in the same region, and reduced spectral contents for subcell current limitation. As a result, the three spectra qualify as Class C simulator according ASTM standard E 927–91, although applied to the range 400–1900 nm range instead of 400–1100 nm.

Although the linearity in the III–V devices considered in this paper is expected to hold [25] and about 2/3 of the solar constant is considered enough as bias light level as established in the standard [26], we looked for spectral conditions as close as possible to standard conditions as design criterion. This criterion tends to assure that the measured *SR* corresponds to the response expected under work conditions. The work of Meusel *et al* [19] shows some influence of using different bias spectra on the measurement conditions, but there is no explanation about it. This influence will be matter of study in a future work.

Table 3 shows a summary of the relative short-circuit currents generated by each subcell when each spectrum is used compared to the theoretical values generated using the AM0 spectrum. Calculations were numerically performed using the SR extracted from [12]. Results obtained show the goodness

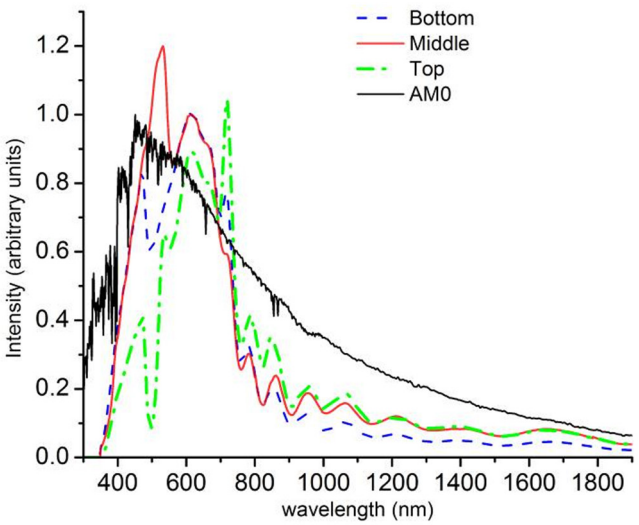

Figure 5. The three bias light spectra used for subcell selection in a 3J cell measurement. The reference indicates the subcell that limits the 3J short-circuit current. The curves are normalized and compared with the AM0 spectrum.

of each spectrum to select the cell of interest by forcing it to limit the current, and also the relative vicinity to AM0 standard operation conditions.

All spectra were tested in the lab using commercial triple junction (3J) cells for space applications. However, it is necessary to take into consideration the possibility of using other spectra because each cell in itself is unique. The conditions found for the commercial 3J subcell selection presented here could fail for other cells having different SR respect to that used in our calculations. Our experience indicates that bias light spectra should be tuned and verified for the particular device under test.

Finally, to end the analysis, the V_{OC} and J_{SC} values measured on a commercial 3J cell using the spectra determined for subcell selection were compared with the nominal values provided by the manufacturer under standard conditions [29]. The results, presented in table 4, show the operating conditions of the cell under the Top and Bottom spectra are very close to those under standard conditions, with a maximum difference in short-circuit current of approximately 13%. In the case of the Middle spectrum the difference is greater reaching approximately 31%, which is consistent with the higher irradiance of the Middle spectrum compared to the other presented above. On the other hand, the open circuit voltage is comparable in the three cases, differing no more than 1.5%.

As commented before, discrepancies are originated in the necessary distinctions created for the current limitation by the subcell chosen in each case, and in some extent by the particular spectral limitations of the dichroic lamps. This fact is evident enough from figure 5, particularly regarding the spectral limitation of the IR components dictated by dichroic lamps, putting the current generation of Bottom cell near of Middle and Top cells. Thus, current limitation of the Top cell is provided by sectioning short wavelength components, while for current limitation of the Middle cell these components are enhanced.

Table 2. Comparison of the spectral distribution for the three spectra for cell selection in 3J cells and the standard AM0.

Wavelength interval (nm)	Top spectrum (% of total)	Mid spectrum (% of total)	Bot spectrum (% of total)	AM0 (% of total)	Top/AM0	Mid/AM0	Bot/AM0
300–400	1.0	1.8	2.4	7.4	0.1	0.2	0.3
400–500	7.1	16.2	16.8	14.8	0.5	1.1	1.1
500–600	17.0	24.1	22.0	14.7	1.2	1.6	1.5
600–700	24.0	22.2	25.7	12.7	1.9	1.8	2.0
700–800	16.1	9.7	12.7	10.1	1.6	1.0	1.3
800–900	7.8	4.6	4.8	8.1	1.0	0.6	0.6
900–1000	5.0	3.7	3.0	6.4	0.8	0.6	0.5
1000–1100	4.5	3.3	2.6	5.3	0.8	0.6	0.5
1100–1200	3.1	2.5	1.8	4.4	0.7	0.6	0.4
1200–1300	2.9	2.4	1.6	3.7	0.8	0.6	0.4
1300–1400	2.4	1.9	1.3	3.1	0.8	0.6	0.4
1400–1500	2.2	1.7	1.2	2.6	0.8	0.7	0.5
1500–1600	1.8	1.5	1.0	2.2	0.8	0.7	0.5
1600–1700	2.2	1.9	1.2	1.9	1.2	1.0	0.7
1700–1800	1.8	1.5	1.0	1.5	1.2	1.0	0.7
1800–1900	1.2	1.0	0.7	1.2	1.0	0.8	0.6

Table 3. Relative short-circuit current generated by each subcell of a 3J for the three spectra showed in figure 5 and the AM0 spectrum. A typical SR, extracted from [12], was used for calculations.

	Short-circuit current			
Spectrum →	AM0	Top	Mid	Bot
Top cell	1	1	1.33	1.63
Middle cell	1.2	1.51	1	1.49
Bottom cell	2	1.4	1.12	1

Table 4. Comparison of the electrical parameters of a 3J cell under the bias spectra with the nominal values provided by the manufacturer.

Spectrum	V_{OC} (V)	J_{SC} (mA cm^{-2})	ΔV_{OC} (%)	ΔJ_{SC} (%)
AM0 (manufacturer)	2.60	17.1	—	—
Top	2.58	17.5	–0.8	1.7
Middle	2.56	22.5	–1.5	30.8
Bottom	2.56	19.4	–1.5	12.7

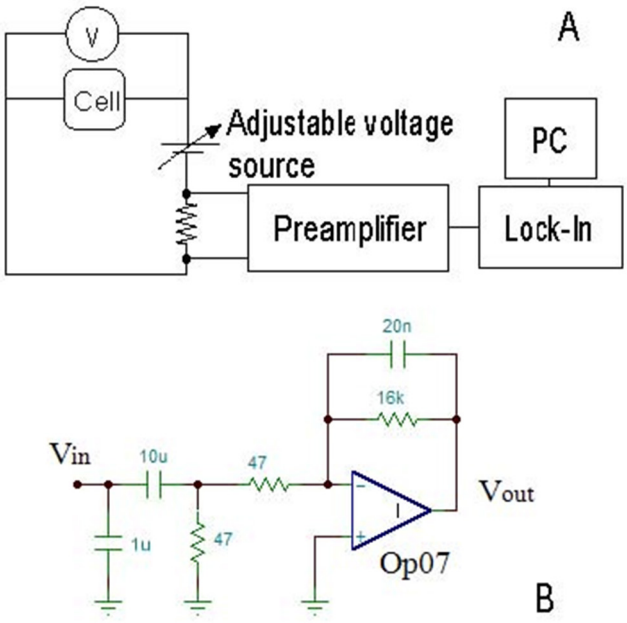

Figure 6. Images showing, (A) scheme of the circuit for electrical bias and signal measurement, (B) details of preamplifier circuit.

3. Electrical setup

3.1. External circuit

The external circuit is composed by a stable resistor R and a home-made variable voltage source. Their combination allows the subcell under test to achieve the short-circuit condition (figure 6(A)). The current photogenerated by the chopped light is sensed through the resistor (acting as current-voltage converter) connected to a homemade pre-amplifier based on a very low noise operational amplifier stage with a low pass filter and capacitive coupling to remove both, high frequencies and DC components (figure 6(B)). The pre-amplifier delivers a voltage proportional to the current flowing through the circuit and then measured by the lock-in amplifier, giving a higher dynamic reserve. In addition, the circuit contains a voltmeter to sense the voltage of the cell under measurement. Tests performed on the setup have shown that the sensitivity of the system is less than 10 nA. The frequency of the chopped light was selected considering low frequency noise and wide-band noise in order to improve the signal-to-noise ratio. To do this, the spectral components of the electrical noise present when there is no signal were analyzed through numerical Fourier transform made on the voltage at the lock-in input. According with the obtained Fourier spectrum, an interval of 700–800 Hz was defined as a region with minor spectral components of noise, and therefore chosen as an appropriate chopper frequency range.

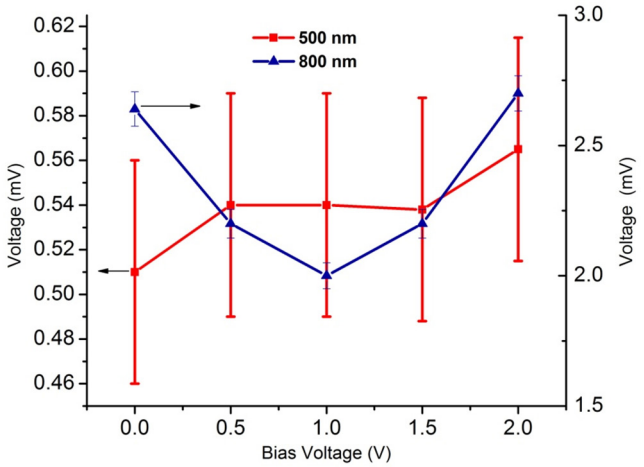

Figure 7. Signal at 500 nm and 800 nm versus bias voltage. Ge subcell is limiting the cell current.

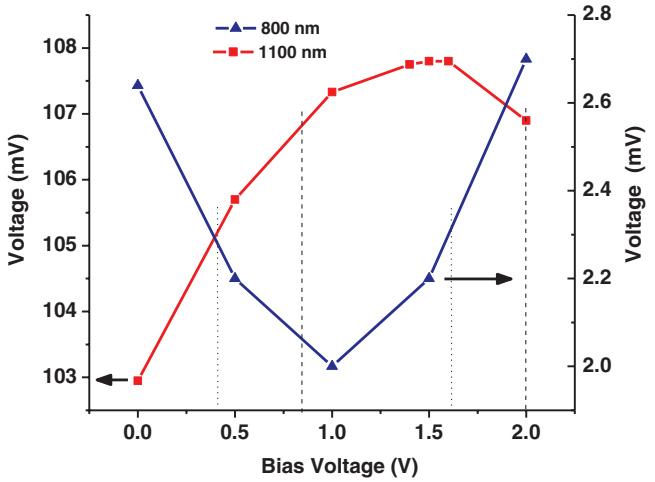

Figure 8. Signal at 1100 nm and 800 nm versus bias voltage. Ge subcell is limiting the cell current. Dotted and dashed lines define the intervals of adopted variability for the 800 nm and 1100 nm signals respectively (see text).

3.2. Voltage bias condition

To achieve the short circuit condition for the subcell to be measured, it is necessary to consider that the three subcells are series connected such that $V_{\text{cell}} = V_{\text{Top}} + V_{\text{Middle}} + V_{\text{Bottom}}$. Thus, when the cell is under short circuit conditions, $V_{\text{cell}} = 0$, the voltage drop on the subcell to be measured is not necessarily equal to 0. For instance, when the bottom subcell limits the current, the two upper subcells (top and middle) work together at a value close to the sum of their open circuit voltages. In consequence, if the external circuit submits the cell at $V_{\text{cell}} = 0$, then the bottom subcell is polarized with $V_{\text{Ge}} = -(V_{\text{GaAs}} + V_{\text{InGaP}})$. However, if the breakdown voltage is very high and the subcells have a high parallel resistance such that they perform as an ideal diode, the measurement can be done by placing the cell voltage equal to zero, $V_{\text{cell}} = 0$. This is usually the case for the GaAs and InGaP subcells in InGaP/GaAs/Ge triple-junction cells. Contrarily, for the Ge subcell in 3J cells, extra attention needs to be spent to submit this subcell to short circuit conditions because it is often not behaved as an ideal diode. A detailed discussion about the problems that can occur in the measurement of SR in multi-junctions, particularly addressed to the Ge subcell, is presented in the paper of Meusel *et al* [19]. The approach to electrically bias the Ge subcell is that once it is selected by the light bias, its SR is minimized by varying the bias voltage of the cell at wavelengths where it is expected to be null.

Figure 7 shows the cell response versus bias voltage at 500 nm and 800 nm, where the Bottom subcell should have no response whatsoever. For 500 nm, the high noise level and very low signal (less than 1 mV, left axis) does not allow visualizing a signal minimum. Considering this result, we also decided to maximize the SR in the wavelength region where the Bottom subcell should have an appreciable response, at 1100 nm. This situation is that stated in the works of Meusel *et al* [19] and Barrigón *et al* [22], where the signal of the Ge subcell increases while the artifact signal is minimized simultaneously. Figure 8 presents both bias voltage responses for 800 nm and 1100 nm where both minimum and maximum signals can be observed. The correct bias voltage is then selected by taking into account both the maximum response at 1100 nm and the minimum response at 800 nm. For both signals at 800 and 1100 nm, different bias voltage ranges are defined according to their measurement errors of ±8% around the minimum and ±1% around the maximum, respectively (estimated errors will be justified in section 4.1). These intervals of 0.4–1.6 V for the minimized signal at 800 nm and 0.85–2.0 V for the maximized at 1100 nm are depicted in figure 8 with vertical dotted lines. From the overlap of both intervals we chose the voltage bias of 1.5 V.

It must be noted that the electrical bias obtained with this method (1.5 V) is somewhat different than the sum of open circuit voltages of the InGaP and GaAs cells of 2.3 V. The origin of such difference could be associated to some large area effects (the cells under study have an area of 27.5 cm^2), as indicate preliminary results we obtained for very tiny devices (area 1 mm^2) where bias voltages for the Ge subcell approaches the estimated 2.3 V from the subcells V_{OC} sum. However, up to now we did not find a consistent explanation for this behavior. It should be stressed that the described procedure to find the proper electrical bias has to be performed for each cell under study.

Recent publications showed there could be an artifact associated to luminescent coupling between InGaP and GaAs subcells in SR measurements when the last subcell is limiting the current [21, 29], and thus a particular electrical bias could be necessary for measuring the GaAs subcell. Our results, presented in section 4, did not show anomalies in this sense, but a careful study could be necessary in other cases. Artifacts associated to the low breakdown voltage of the Ge cell [22] neither were found.

3.3. Automation

Both filter wheels are moved by two stepper motors commanded by a dedicated software developed in Visual Basic through the PC parallel port. A transistorized driver was constructed to control the motors. The software also communicates

with the lock-in amplifier throughout the RS-232 interface reading the voltage values from the amplifier.

To improve the signal/noise ratio we introduced an appropriate averaging algorithm. For each wavelength, four sets of 10 signal values are acquired and the dispersion of the mean value of each set is calculated and compared with a critical value previously defined, that may be higher or lower depending on the quality of signal. If this dispersion does not meet this quality criterion, the lock-in integration constant is increased until the critical value is met. Then, the last 40 values are averaged and the root mean square (RMS) error is calculated to give the signal value at that wavelength. Using this procedure, each measurement from 300 nm to 1900 nm is performed reliably and automatically. Finally, the software shows the complete SR of each subcell on the screen, after taking a complete reading of the cell and reference values. All the measurement procedure, except for the bias light filters change, is made automatically.

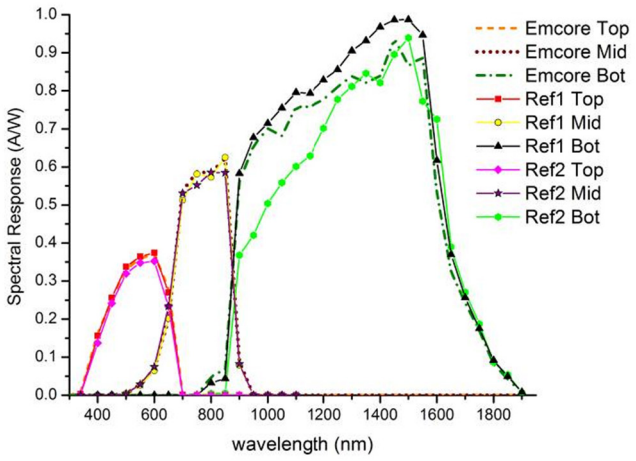

Figure 9. SR measurements of two secondary reference cells using as primary reference a calibrated ATJ cell provided by emcore corp. (also shown).

4. First measurements and results

4.1. Transference of the SR primary standard

All the measurements are performed at controlled temperature (25 °C), using a commercial thermostatic plate. Two 3J cells were integrated in an appropriate support for robustness handling and were calibrated as secondary reference cells using a calibrated ATJ (advanced triple junction) cell provided by Emcore Corp. (nowadays SolAero Technologies) as the primary standard. The first cell (Ref1) is a flight qualified cell and the second one (Ref2) is a non-flight (of poor electrical characteristics) cell. The averaged results from several measurements for the InGaP/GaAs/Ge subcells of secondary and primary cells are shown in figure 9. The SRs show differences centered at the Ge subcell wavelength response region. The Ref2 has a poor response at shorter wavelengths, while Ref1 presents the highest response altogether. The Emcore primary standard response for the Ge subcell lies in the middle of Ref1 and Ref2. The Ref2 is considered as a cell that does not have the electrical characteristics suitable for integration into a flight solar panel (classified as 'Low Electrical' by the provider), and this is clearly visible in the poor Ge subcell SR, likely associated to problems in the semiconductor layers epitaxy. In the case of Ref1, the response of the Ge subcell is the highest because it is a CIC (covered and interconnected cell) assembly, where the coverglass and the Emcore ATJ cell conform an optimized antireflection structure as a whole. This fact is also reflected in the top and middle subcells response enhancement for Ref1.

The error value in the calibration of the secondary reference cells cannot be calculated based on the primary cell calibration errors because those were not provided by the manufacturer. Thus, we assumed an error of three times the standard deviation (99.7% confidence interval) calculated from several measurements. The results showed that in the zone where each subcell is sensitive (400–650 nm for Top, 550–850 nm for Middle, and 800–1800 nm for Bottom), the error varies around 1%–3%, and then increases to almost 8% near the cut-off wavelength of each subcell (see figure 10). This error boost near the cut-off response of each subcell is a consequence of the reduced signal/noise ratio at the edges, which produces a higher variability of the final read value of the SR.

The previous analysis is based on the variability of the measurement induced by random fluctuations. As commented in the section 1, there are several error sources associated to the SR measurement as detailed in [10]. Some of them, like the ones associated to the *I–V* converter and lamp ageing, are avoided by using a reference cell on each measurement. Resistance thermal drift is minimized due to the measurement of cells that produce very similar currents; the automation measurement procedure inserted in the code provides the best lock-in scale and time constant, so errors associated are also minimized; cell temperature is controlled along the measurement; spatial uniformity of monochromatic and bias light were set into the limits of the standard [26] and light beams cover all the device surface. Also, filters transmittance are periodically checked.

Those sources associated to pronounced function variation, as produced in band edges or interference patterns in the SR, were numerically evaluated using a similar concept as that applied in [15], but considering our particular method for measuring the SR. In order to assess the error introduced by the method, the following procedure was applied. For a given and known SR (for instance the SR used as primary reference), the *measurement process is simulated* doing the integral of the QTH lamp spectrum (monochromatic light source), the narrow-band filter transmittance (for a given central wavelength λ), and the SR, which gives the current density generated at this λ (equation (2)) and then divided by the SR(ref) as established in equation (1). The error is then *estimated* through the differences between original SR values and those simulated for a given λ. This methodology was applied to selected wavelengths in order to evaluate the method at different scenarios, i.e. band edge (for instance at 850 nm and 900 nm, for GaAs and Ge subcells), central band (at 750 nm

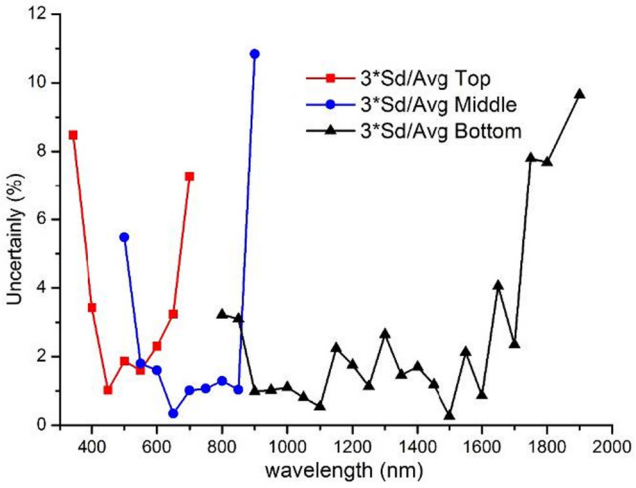

Figure 10. SR error estimated using several measurements.

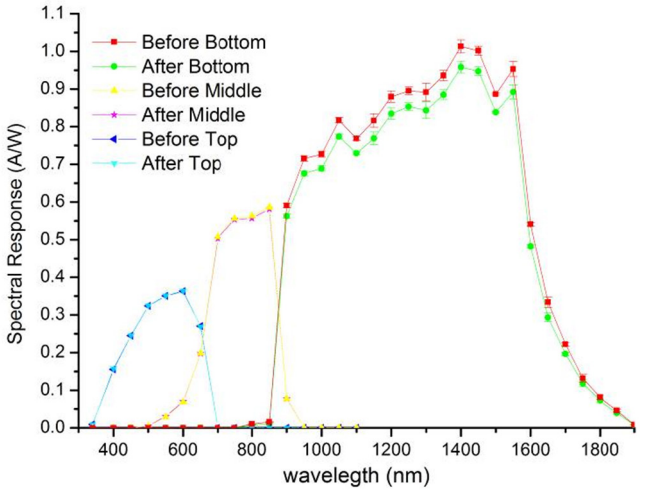

Figure 11. SR of an ATJ cell before and after irradiation with 10 MeV protons.

for GaAs subcell), and vicinities of a visible interference pattern (1400, 1450, and 1500 nm for Ge subcell). We found the larger errors appear for the band edges, with figures as large as 25%, while the worse case associated to interference variations was less than 2%. However, the possible variability of the SR values at the edges produces a negligible effect on the SR integral, due to the inherently small values of SR at the edges. This fact was verified by calculating the integrals of SR for the 'true' values for the edges and using these values modified by the error: differences in the integral were in the order of 1%.

As commented before, we did not notice artifacts associated to luminescent coupling for the GaAs subcell SR in our experimental conditions. In the work of Lim *et al* [30] a clear dependence on the bias voltage of GaAs SR originated in the luminescent coupling of InGaP and GaAs subcells is presented, artifact characterized by a less than expected *SR* in the range 600–900 nm and higher than expected in 400–600 nm. Figure 9 exhibits a normal GaAs SR for our measurements, fully compatible with the reference calibration values provided by Emcore.

4.2. Evaluation of radiation damage

The DES of CNEA performs research activities focused on radiation damage of solar cells [2, 8]. Particularly, some tests of radiation damage on triple-junction Emcore ATJ cells were performed. In this frame, SR of ATJ cells were measured before and after irradiation with 10 MeV protons by the heavy ion tandem accelerator, TANDAR, at CNEA.

The results of the SR measurements before and after irradiation using a final fluence of 3.08×10^{10} p cm^{-2} are shown in figure 11. The Top and Middle subcells show no appreciable differences before and after irradiation, but the SR of the Bottom subcell shows some degradation after irradiation. It must be mentioned that the measurements were performed several days after irradiation, to allow nuclear activation of the cell materials to decay enough in order to avoid health risk. It is possible that some of the damage could be reversed during that time.

10 MeV proton irradiation produced a measurable degradation in the SR of the Ge subcell. The SR differences in this subcell before and after irradiation are close to 5 % in the central region of the subcell response, higher than the estimated errors. Although it is hard to find specific literature that discusses the effect of 10 MeV proton irradiation on each MJ subcell using the relatively low fluence considered here, the Ge subcell appear to present less resistance to radiation damage in this conditions respect to InGaP and GaAs cells [31]. The results obtained in this work cannot be compared directly with those found in the literature because the experimental conditions and the cells tested are not the same.

5. Conclusions

The development of an experimental setup to perform SR measurements on monolithic multijunction cells have concluded successfully. One of the main aspects of this work is the achievement of suitable bias light conditions in the selection of the subcell of interest using a low cost approach based on commercial dichroic lamps and bandpass interference filters. As a result, three spectral conditions that submit the subcells of InGaP/GaAs/Ge 3J cells under near work standard conditions were found and verified. The electrical bias of the Ge subcell in an InGaP/GaAs/Ge triple junction structure was also studied, and the maximization of the Ge 1100 nm signal was identified as an appropriate parameter to define the bias voltage.

For the case of commercial cells, the measurement random errors were evaluated and estimated with an uncertainty of 1%–3% into the sensitive range of each subcell, while near the cut-off wavelengths it increases up to 10%. The systematic error associated to the method employed here was estimated as 25% maximum for edges band and less than 2% in central bands. The generalized diminished uncertainties enables observation of minor changes in the SR of cells allowing to assess small radiation damage effects or small changes produced by other factors.

Acknowledgments

The authors acknowledge the collaboration of C G Bolzi and L Gonzalez in the integration of the reference cells. The critical reading of this paper performed by M D Perez is also acknowledged. This development was carried out in the frame of a cooperation agreement between the Argentine National Atomic Energy Commission (CNEA) and the Argentine National Commission for Space Activities (CONAE), which is addressed in these stages to SAOCOM and SAC-D satellites. J García was supported by a CONICET doctoral fellow. This work was funded by CNEA, CONAE, and the grants PIP2009-2011 Nº 02318 and PIP2012-2014 Nº 01052 (CONICET), and PICT2007 Nº 01143 and PICT2013 Nº 3077 (ANPCyT).

References

[1] Bolzi C G *et al* 2002 First experiment of argentine solar cells in space: modules fabrication, characterisation, and telemetry data analysis from SAC-A satellite *Sol. Energy Mater. Sol. Cells* **73** 269
[2] Alurralde M *et al* 2004 Experimental and theoretical radiation damage studies on crystalline silicon solar cells *Sol. Energy Mater. Sol. Cells* **82** 531
[3] Plá J, Barrera M and Rubinelli F 2007 Influence of the InGaP window layer on the optical and electrical performance of GaAs solar cells *Semicond. Sci. Technol.* **22** 1122
[4] Barrera M, García J, Socolovsky H, Rubinelli F, Godfrin E and Plá J 2008 Activities on simulation and characterization of multijunction solar cells for space applications in Argentina *Proc. 23rd European Photovoltaic Solar Energy Conf. Exhibition (Valencia)* p 781
[5] Alurralde M *et al* 2009 Flight models for the Aquarius/SAC-D satellite mission *Proc. 24th European Photovoltaic Solar Energy Conf. (Hamburg)* p 695
[6] Socolovsky H, Yaccuzzi E, Godfrin E M and Plá J 2011 On the illumination spectrum influence in the electrical characterization of multijunction solar cells *Proc. 26th European Photovoltaic Solar Energy Conf. (Hamburg)* p 795
[7] Barrera M, Rubinelli F, Rey-Stolle I and Plá J 2012 Numerical simulation of Ge solar cells using D-AMPS-1D code *Physica* B **407** 3282
[8] Alurralde M *et al* 2013 Development of solar arrays for argentine satellite missions *Aerosp. Sci. Technol.* **26** 38
[9] Ebner B, Agostinelli G and Dunlop E 2000 Automated absolute spectral response characterisation for calibration of secondary standards *Proc. 16th European Photovoltaic Solar Energy Conf. (Glasgow)* p 2203
[10] Emery K, Dunlavy D, Field H and Moriarty T 1998 Photovoltaic spectral responsivity measurements *Proc. 2nd World Conf. Photovoltaic Solar Energy Conversion (Vienna)* p 2298
[11] Winter S, Metzdorf J and Fernandez Lisbona E 2004 Spectral responsivity calibration of Ge component solar cells derived from triple junction devices *Proc. 19th European Photovoltaic Solar Energy Conf. Exhibition (Paris)* p 2544
[12] King D L, Hansen B R, Moore J M and Aiken D J 2000 New methods for measuring performance of monolithic multi-junction solar cells *Proc. 28th IEEE Photovoltaic Specialists Conf. (Anchorage)* p 1197
[13] Rodríguez J A, Fortes M, Alberte C, Vetter M and Andreu J 2013 Development of a very fast spectral response measurement system for analysis of hydrogenated amorphous silicon solar cells and modules *Mater. Sci. Eng.* B **178** 94–8
[14] Pravettoni M, Komlan A, Galleano R, Müllejans E D and Dunlop H 2011 An alternative method for spectral response measurements of large area thin film photovoltaic modules *Prog. Photovolt., Res. Appl.* **20** 416–422
[15] Field H 1997 Solar cell spectral response measurement errors related to spectral band with and chopped light waveform *Proc. 26th IEEE Photovoltaic Specialists Conf. (Anaheim)* p 471
[16] Virshup G F and Werthen J G 1985 Spectral response measurements of two-terminal multijunction solar cells *Proc. 18th IEEE Photovoltaic Specialists Conf. (New York)* p 618
[17] Burdick J and Glatfelter T 1986 Spectral response and *I–V* measurements of tandem amorphous-silicon alloy solar cells *Sol. Cells* **18** 301–14
[18] Heidler K, Schönecker A, Müller-Bierl B and Bücher K 1991 Progress in the measurement of multi-junction devices at ISE *Proc. 22nd IEEE Photovoltaic Specialists Conf. (Las Vegas)* p 430
[19] Meusel M, Baur C, Bett A W, Warta W and Fernández E 2003 Spectral response measurements of monolithic GaInP/Ga(In)As/Ge triple-junction solar cells: measurement artifacts and their explanation *Prog. Photovolt., Res. Appl.* **11** 499–514
[20] Haverkamp E J, Bauhuis G J, Bissels G M M W, Mulder P and Schermer J J 2007 Multijunction spectral response measurements setup based on high power LEDs for subcell selection *Proc. 22nd European Photovoltaic Solar Energy Conf. Exhibition (Milan)* p 276
[21] Steiner M A and Geisz J F 2012 Non-linear luminescent coupling in series-connected multijunction solar cells *Appl. Phys. Lett.* **100** 251106
[22] Barrigón E, Espinet-González P, Contreras Y and Rey-Stolle I 2015 Implications of low breakdown voltage of component subcells on external quantum efficiency measurements of multijunction solar cells *Prog. Photovolt., Res. Appl.* **23** 1597–607
[23] Socolovsky H, García J and Plá J 2010 Setup development for spectral response measurement on multijunction solar cells *Proc. 25th European Photovoltaic Solar Energy Conf. Exhibition (Valencia)* p 854
[24] Benjamin K D, Armitage A F and South R B 2006 Harmonic errors associated with the use of choppers in optical experiments *Measurement* **39** 764–70
[25] Emery K, Meusel M, Beckert R, Dimroth F, Bett A and Warta W 2000 Procedures for evaluating multijunction concentrators *Proc. 28th IEEE Photovoltaic Specialists Conf. (Anchorage)* p 1126
[26] ASTM Standard E1021-12 2012 Standard test method for spectral responsivity measurements of photovoltaic devices
[27] ASTM Standard E 490 – 00a(2014) 2014 Solar constant and zero air mass solar spectral irradiance tables
[28] ASTM Standard E927-10(2015) 2015 Standard specification for solar simulation for terrestrial photovoltaic testing
[29] http://solaerotech.com/wp-content/uploads/2015/03/ATJ-Datasheet.pdf
[30] Lim S H, Li J-J, Steenbergen E H and Zhang Y-H 2013 Luminescence coupling effects on multijunction solar cell external quantum efficiency measurement *Prog. Photovolt., Res. Appl.* **21** 344–50
[31] Imaizumi M, Takamoto T, Sumita T, Ohshima T, Yamaguchi M, Matsuda S, Ohi A and Kamiya T 2003 Study of radiation response on single-junction component sub-cells in triple-junction solar cells *Proc. 3rd World Conf. Photovoltaic Solar Energy Conversion (Osaka)* p 599